$\delta_{MeV}^{(N)} = F_{MeV}^{(N)}/F_{MeV}^{(max)} = 0.57 \pm 0.11$ and $\delta_{MeV}^{(S)} = F_{MeV}^{(S)}/F_{MeV}^{(max)} = 0.54 \pm 0.09$, respectively. The model calculations of leakage neutrons indicate (*1*) that these deficits may correspond to about 5% by weight of water in a homogeneous subsurface layer. This value is larger than the 0.1% by weight of absorbed water estimated to be in the soil as a result of atmospheric humidity (*16*). The higher content may be associated with chemically bound water in the subsurface.

The map of neutrons at 3.4 to 7.3 MeV agrees with the dichotomy boundary of martian topography (*12*). The low flux of 3-MeV neutrons in the north cannot be explained by the northern winter CO_2 frost, because it does not change the leakage flux at MeV energies (*6*). Thus, Mars has two large provinces—one in the northern lowlands and the other in the southern highlands—with an uppermost subsurface layer containing hydrogen, and this hydrogen may be bound in water ice. A global mechanism of water transport for the surface and the subsurface may be needed to explain the presence of subsurface water ice at low elevation in the north and high elevation in the south [e.g., see (*17*)].

Another difference between the two maps (Figs. 1 and 2) is that the southern province has a much lower flux of epithermal neutrons relative to the flux for neutrons at 3.4 to 7.3 MeV range. The ratio between the observed deficits is $\eta = \delta_{eth}^{(S)}/\delta_{MeV}^{(S)} = 0.31$. The model of a homogeneous layer indicates that the water-produced deficit of neutrons is about the same at epithermal and 3-MeV energy ranges (*6*). Neutrons at MeV energies leak from shallower depths than do epithermal neutrons (*8*). Therefore, the stronger decrease of epithermal particles in the southern province may result from a layered structure of the subsurface, in which a dryer upper layer of soil with about 5% water (which contributes mainly to MeV neutron emission) covers a wetter, lower layer with a higher percentage of water ice (which makes the main contribution to epithermal neutron emission).

To illustrate this possibility, we produced a numerical model of the layered subsurface, which describes the additional lower flux of epithermal neutron leakage. An icy layer with thickness $h_0 = 20$ cm was positioned in the subsurface below a layer of dryer soil with 5% water and a variable thickness h. The icy layer produces additional deficits of leakage neutrons $\delta_{eth}^{(S)}(h)$ and $\delta_{MeV}^{(S)}(h)$ in comparison with values $\delta_{eth}^{(S)}(\infty)$ and $\delta_{MeV}^{(S)}(\infty)$, which correspond to the upper layer of soil only, when $h = \infty$. The additional deficit disappears when thickness h increases (Fig. 3). The observed ratio $\eta = \delta_{eth}^{(S)}/\delta_{MeV}^{(S)} = 0.31$ is consistent with the thickness of an upper layer of soil about 10 to 60 cm above the top of an icy layer (Fig. 3). This model is just one of many that is consistent with these observations [see also (*15*)]; however, $h_0 = 20$ cm is close to the minimal thickness of a water ice layer that may fit the observations.

References and Notes

1. M. C. Malin, K. S. Edgett, *Science* **288**, 2330 (2000).
2. B. M. Jakosky, R. J. Phillips, *Nature* **412**, 237 (2001).
3. H. H. Kieffer *et al*., *Science* **194**, 1341 (1976).
4. M. T. Zuber *et al*., *Science* **282**, 2053 (1998).
5. D. E. Smith *et al*., *Science* **284**, 1495 (1999).
6. D. M. Drake, W. C. Feldman, B. M. Jakosky, *Proc. Lunar Planet. Sci. Conf.* **17**, 186D (1986).
7. W. C. Feldman *et al*., *J. Geophys. Res.* **98**, 20855 (1993).
8. J. Masarik, R. J. Reedy, *J. Geophys. Res.* **101**, 18891 (1996).
9. W. V. Boynton *et al*., in preparation.
10. R. S. Saunders, AGU Fall Meeting 2001, abstract #P41A-08 (American Geophysical Union, Washington, DC, 2001).
11. The circular orbit of the mapping stage does not allow us to distinguish the local background from the spacecraft from the constant component of the martian neutron emission. During the elliptical orbits with period about 10 hours, the solid angle of Mars $\Delta\Omega$ varied from 4.8 steradians in periapsise down to 0.1 steradian in apoapsise. The local background due to galactic cosmic rays depends on the fraction of the open sky $(4\pi - \Delta\Omega)/4\pi$, whereas the signal from Mars is proportional to $\Delta\Omega$.
12. In addition to the cosmic ray–induced local background, Odyssey affects the background signal by scattering and absorption of neutrons from Mars. This effect will be removed when present maps of counts of neutrons are transformed into corrected maps of neutron emission of the surface of Mars. This effect may not produce any coordinate-dependent variations of detected counts on the orbit, but it should be taken into account for evaluation of absolute values of surface flux.
13. D. E. Smith *et al*., *J. Geophys. Res.* **106**, 23689 (2001).
14. W. C. Feldman *et al*., *Science* **297**, 75 (2002); published online 30 May 2002 (10.1126/science.1073541).
15. W. V. Boynton *et al*., *Science* **297**, 81 (2002); published online 30 May 2002 (10.1126/science.1073722).
16. D. Möhlman, Proceedings of Workshop, Potsdam, Germany, 17 to 19 April 2002.
17. V. R. Baker, *Nature* **412**, 228 (2001).

18. We thank the Odyssey project team, which made these space measurements possible, as well as the anonymous reviewers for useful questions and comments.

6 May 2002; accepted 22 May 2002
Published online 30 May 2002;
10.1126/science.1073616
Include this information when citing this paper.

Distribution of Hydrogen in the Near Surface of Mars: Evidence for Subsurface Ice Deposits

W. V. Boynton,[1]* W. C. Feldman,[2] S. W. Squyres,[3] T. H. Prettyman,[2] J. Brückner,[4] L. G. Evans,[5] R. C. Reedy,[2,6] R. Starr,[7] J. R. Arnold,[8] D. M. Drake,[9] P. A. J. Englert,[10] A. E. Metzger,[11] Igor Mitrofanov,[12] J. I. Trombka,[13] C. d'Uston,[14] H. Wänke,[4] O. Gasnault,[14] D. K. Hamara,[1] D. M. Janes,[1] R. L. Marcialis,[1] S. Maurice,[15] I. Mikheeva,[1] G. J. Taylor,[16] R. Tokar,[2] C. Shinohara[1]

Using the Gamma-Ray Spectrometer on the Mars Odyssey, we have identified two regions near the poles that are enriched in hydrogen. The data indicate the presence of a subsurface layer enriched in hydrogen overlain by a hydrogen-poor layer. The thickness of the upper layer decreases with decreasing distance to the pole, ranging from a column density of about 150 grams per square centimeter at –42° latitude to about 40 grams per square centimeter at –77°. The hydrogen-rich regions correlate with regions of predicted ice stability. We suggest that the host of the hydrogen in the subsurface layer is ice, which constitutes 35 ± 15% of the layer by weight.

There is ample evidence that water has been important in shaping the martian surface (*1*, *2*) and that water is present on Mars today in the north polar residual cap (*3*). In more recent times, water may have flowed over the surface to form gullies (*4*), and ice may have been lost from zones of dissected duricrust (*5*).

Here, we report the presence of near-surface ice at two locations on Mars based on the determination of the depth dependence of hydrogen abundances in the upper meter of the martian regolith. The measurements were made with the Gamma-Ray Spectrometer (GRS) (*6*, *7*) on the Mars Odyssey mission. The GRS is a collection of three instruments used to determine the elemental composition of the martian surface. The instruments are the Gamma Subsystem, the Neutron Spectrometer, and the High Energy Neutron Detector. Data from the two neutron instruments are reported separately (*8*, *9*). Here, we integrate the neutron data from (*8*) with the gamma-ray data and make quantitative estimates of the hydrogen distribution in the regolith and its implications for water-ice abundances.

The techniques of gamma-ray and neutron spectroscopy have been discussed in detail elsewhere (*10*, *11*). They rely on cosmic-ray particles, mostly protons and alpha particles with energies of a few GeV, as the excitation source. When cosmic rays strike the atmosphere and surface of Mars, they generate neutrons from other nuclei by various nuclear reactions. The neutrons then lose energy by collision with surrounding nuclei, and in the process they excite other nuclei, which then de-excite by emission of gamma rays. After the neutrons approach thermal energies, they can be captured by nuclei, which then also de-excite by emission of gamma rays. Some of the neutrons escape the planet's surface and can be detected in orbit. The flux of these leakage neutrons is indicative of the amount of moderation and capturing of the neutrons. These processes are a function of the composition of the surface and atmosphere because different elements have different cross sections for capture and have different abilities to moderate neutrons. Hydrogen is especially effective at moderating neutrons because its mass is nearly the same as that of the neutron.

[1]Lunar and Planetary Laboratory, University of Arizona, Tucson, AZ 85721, USA. [2]Los Alamos National Laboratory, Los Alamos, NM 87545, USA. [3]Center for Radiophysics & Space Research, Cornell University, Ithaca, NY 14853, USA. [4]Max-Planck-Institut für Chemie, 55020 Mainz, Federal Republic of Germany. [5]Science Programs, Computer Sciences Corporation, Lanham, MD 20706, USA. [6]Institute of Meteoritics, University of New Mexico, Albuquerque, NM 87131, USA. [7]Department of Physics, The Catholic University of America, Washington, DC 20064, USA. [8]Department of Chemistry, University of California San Diego, La Jolla, CA 92093, USA. [9]TechSource, Sante Fe, NM 87505, USA. [10]Victoria University of Wellington, Wellington, New Zealand. [11]Jet Propulsion Laboratory, California Institute of Technology, Pasadena, CA 91109, USA. [12]Space Research Institute, Moscow, Russia. [13]NASA/Goddard Space Flight Center, Greenbelt, MD 20771, USA. [14]Centre d'Etude Spatiale des Rayonnements, Toulouse, France. [15]Observatoire Midi-Pyrenees, 31400 Toulouse, France. [16]University of Hawaii, Honolulu, HI 96822, USA.

*To whom correspondence should be addressed. E-mail: wboynton@lpl.arizona.edu

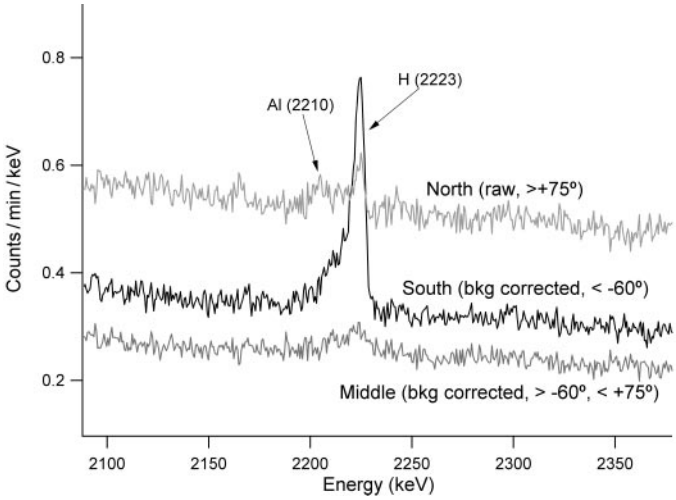

Fig. 1. Portions of the Odyssey gamma-ray spectra showing the emission line due to capture of thermal neutrons by hydrogen. The boom on which the gamma sensor is located has not yet been erected, so we get a small background contribution from hydrogen in the spacecraft. Spectra accumulated over the region in the northern latitudes are used to generate a spacecraft background spectrum, as this region is covered by a thick CO_2 frost that is nearly opaque to gamma rays (*24*). bkg, background.

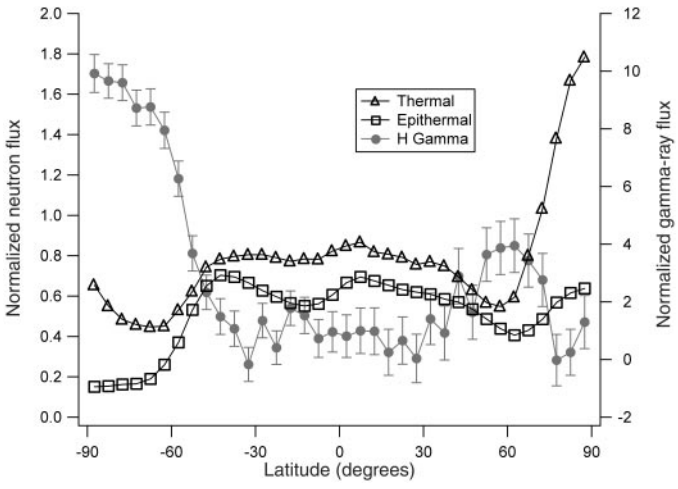

Fig. 2. Normalized fluxes of neutrons and H gamma rays versus latitude. The data are averaged over longitudes 90° to 210°E. These longitudes were chosen to be as far as possible from the residual CO_2 cap in the south, which could have a major effect on the flux of thermal neutrons, similar to that observed in the north due to the seasonal CO_2 frost. The increase in H gamma-ray emission south of about −45° is clearly evident, as is an enrichment in the north. The enrichment in the north does not continue to the pole because the north polar region is currently covered by a thick seasonal CO_2 cap. Note the anticorrelation between the H gamma-ray flux and the epithermal neutron flux.

The flux of both neutrons and gamma rays are affected by the subsurface composition of the regolith, but they have a different dependence on depth. The median depth from which the gamma-ray signal is detected occurs at a column density of about 20 g/cm^2, but if the H concentration is enriched at depth, the median depth is greater. Neutrons are conventionally divided into three different energy bands: fast, epithermal, and thermal (*11*). The fast neutrons that escape to orbital altitudes have a depth dependence comparable to that of the gamma rays, but they do not convey as much information relevant to the distribution of H and will not be used in this work. The epithermal and thermal neutrons are sensitive to depths two or three times greater than the depth for gamma rays.

The GRS returns several neutron spectra and a gamma spectrum about every 20 s, which is the equivalent of one degree of motion or 59 km over the surface. The data are then binned over regions of interest to improve statistics. The emission line from hydrogen is readily apparent in the spectrum from the south polar region (Fig. 1), but the hydrogen signal in the mid-latitudes is nearly absent. For this work, we have binned the data in 5° latitude bands over longitudes from 90° to 210°E (Fig. 2). For most of the planet, the hydrogen gamma signal is very small, but in the south a clear increase is seen with decreasing distance to the pole. This increase toward the south pole is correlated with a reduction in epithermal neutron flux, which independently indicates an increase in H (*8*, *9*).

Relating these data to the distribution of H in the surface is not straightforward. If the flux of neutrons is constant and an element is uniformly distributed with depth, then the concentration of the element is directly proportional to the gamma signal strength. For the case of H, which has a major effect on the thermal neutron flux and whose concentration can vary with depth, the relation between concentration and gamma signal is complex. Here we used a Monte Carlo code, MCNPX (*12*, *13*), to calculate the expected neutron and gamma signal strength for a variety of one- and two-layered regolith models with different atmospheric thicknesses to account for variations due to topography. For all models, we assumed the concentration of elements other than H was that of the soil measured by the Mars Pathfinder Alpha Proton X-Ray Spectrometer (*14*). We then normalized the results to unity for a soil with the equivalent of 1% H_2O by weight.

For models of homogeneous regoliths with varying amounts of H_2O, the epithermal neutron flux decreases monotonically with increasing H_2O content (Fig. 3). The thermal neutron flux, by contrast, first increases as the

H_2O content increases up to about 10% by weight, after which the flux then decreases as the H_2O content continues to increase. This variation in the thermal flux occurs because H is a very effective moderator of neutrons, essentially converting epithermal neutrons into thermal neutrons. At high H content, however, the thermal flux decreases due to capture of the thermal neutrons by H nuclei. In the layered model, the thermal flux decreases rather than increases as the H_2O-poor upper layer gets thinner; it increases again after reaching a minimum at a thickness (column density) of around 60 g/cm^2. The thermal flux decreases because the large H content of the subsurface layer acts as a sink to remove the thermal neutrons that diffuse down from the low-H surface layer. The fact that we see a correlated decrease in the thermal and epithermal neutron flux south of −42° (Fig. 2) indicates that the regolith is layered with a greater H_2O content below the surface.

To quantify this conclusion, we present several different two-layer models (Fig. 4) and compare them with the observed neutron fluxes. The data from the neutron spectrometer have been normalized to 1% H_2O by weight at the location of the Viking 1 landing site (*15*, *16*). Beginning at −42° latitude, as the distance to the south pole decreases, both the thermal and epithermal neutron fluxes decrease together until about −60° latitude, where the thermal flux plateaus and then begins to increase. The data agree with the model calculations, and the deviations almost certainly indicate that the actual distribution of H in the regolith is more complex than our model of two homogeneous layers with a sharp boundary. The data are also consistent with the upper layer having an H_2O content of about 1% by weight near −42° latitude and increasing to 2% near −62°. The exact value of the H_2O content at the surface is dependent on the normalization to the Viking 1 region and is thus not an independent determination. The data are also consistent with the lower layer having an H_2O content of 35 ± 15% by weight, but this determination is not strongly dependent on the normalization value.

The gamma-ray flux values, after background correction, have been normalized to the equivalent of 1% H_2O between +30° and −30° latitude and between 90° and 210°E longitude (*17*). Because the H gamma rays are less sensitive to the composition at depth than the neutrons, a comparison of thermal neutron flux to H gamma-ray flux (Fig. 5) can be used to distinguish H concentrations as the upper layer gets thinner. Here the data suggest that the H_2O content of the lower layer is closer to the upper range of 35 to 50% by weight.

A similar H-rich region is observed in the north. Like the region in the south, it begins to be visible at about 45° latitude (Fig. 2). This region presumably continues to higher latitudes, but it is obscured due to the seasonal CO_2 cap beginning at about 60° latitude. The unobscured data do not go far enough toward the pole to determine whether the H_2O distribution is similar to that of the south.

Some obvious sources of error need to be discussed. We have an instrument with a spatial footprint on the order of 10° (600 km) for gamma rays and epithermal neutrons, and one that is somewhat larger for thermal neutrons. The spatial resolving power is, however, sufficient to rule out a step-function change in H_2O distribution. The data have

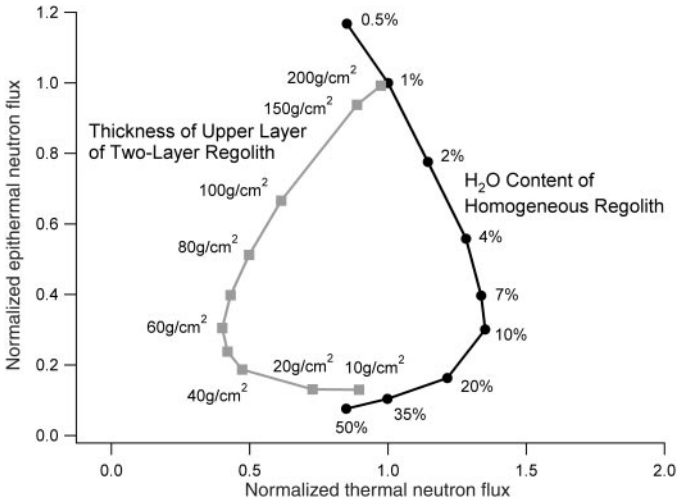

Fig. 3. Calculated epithermal neutron flux versus thermal neutron flux for two different models of the martian regolith. The right curve shows the variation for homogeneous-regolith models with different H_2O contents. The left curve shows the variation for two-layer models in which the upper layer has 1% H_2O, the lower layer has 35% H_2O, and the thickness of the upper layer varies as shown (in units of column density).

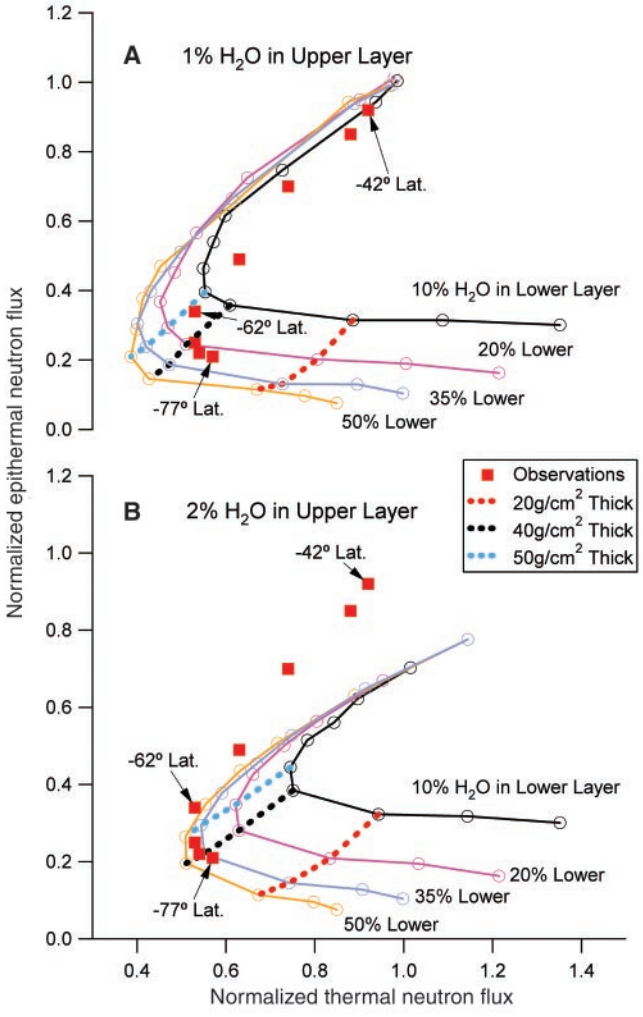

Fig. 4. Calculated and observed epithermal neutron flux versus thermal neutron flux for a family of Mars regolith models. The calculations are for different two-layer models similar to the example in Fig. 3. (**A**) 1% H_2O in the upper layer. (**B**) 2% H_2O in the upper layer. The solid lines connect models with the same H_2O contents in the lower layers (labeled at each end of the lines); the dashed lines connect models with the same depth to the lower layer. Observed fluxes at different latitudes are plotted as unconnected squares. The two most southerly points are not plotted, because they may have some contamination from the high thermal flux of the permanent CO_2 cap. The observations agree well with a model that has 35 ± 15% H_2O in a lower layer and 1 to 2% H_2O in an upper layer that gets thinner at more poleward latitudes (from a column density of about 150 g/cm^2 at −42° to about 40 g/cm^2 at −77°).

been normalized because we have not yet fully validated our absolute calibration of instrument response nor have we determined the strength of the cosmic-ray excitation flux. With the current normalization, we find an implied H_2O content in the driest part of Mars to be about 0.25% by weight. The Viking 1 landing site could not have much less than 1% H_2O, or we would have gotten negative H_2O contents at this driest point. If the Viking 1 site has more H_2O, we would get an increase in the amount of H_2O in the lower layer. Thus our conclusion of around 35% H_2O by weight in the lower layer is robust. Lastly, we have assumed that the composition of the soil with respect to elements other than hydrogen is constant everywhere and is as found by Mars Pathfinder (*14*). The effect of having a different composition in the soil is biggest for elements whose variation would have the biggest effect on the total neutron macroscopic cross section. Here it is chlorine, but twofold variation in the chlorine content of the model soil had only a minor effect on our estimation of the amount of H_2O in either layer. We have looked only at simple models to explain our observations. Although the data are consistent with these models, none of these solutions is unique, and the real H_2O distribution is probably more complicated.

The identification of large quantities of hydrogen in the near surface is unambiguous, but the chemical form in which it is present is not clear. In the upper layer, it is likely that the H is present in the form of physically or chemically bound H_2O, and this layer may be indistinguishable from the soil at mid-latitudes, where ice is not stable. For the lower layer, however, ice may be the only reasonable phase to associate with this much H for several reasons. First, the large amounts of hydrogen, 35 ± 15% H_2O equivalent, is too much to be accommodated by alteration of most rock-forming minerals. Second, the stratification of H into layers with over a 10-fold difference in concentration seems hard to sustain unless a volatility comparable to that of ice is responsible. Third, the H-rich regions are only found in the colder regions, suggesting a strong volatility dependence similar to that expected for ice. Many theoretical studies have predicted regions where H_2O ice should be stable on Mars (*18–20*). Our map of epithermal neutron flux (*8*) shows consistency between regions where ice is expected to be stable at a depth of 80 cm (*21*) and regions of low epithermal flux (Fig. 6).

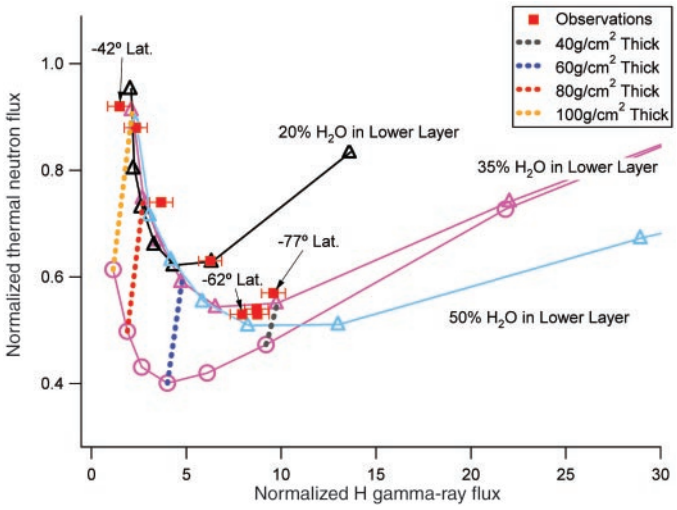

Fig. 5. Calculated and observed normalized thermal neutron flux versus normalized H gamma-ray flux. Circles, calculated models for 1% H_2O in the upper layer; triangles, calculated models for 2% H_2O in the upper layer. The observations are consistent with the model in Fig. 4 at lower latitudes, but they suggest the H_2O content of the lower layer is closer to the upper range from 35 to 50% H_2O.

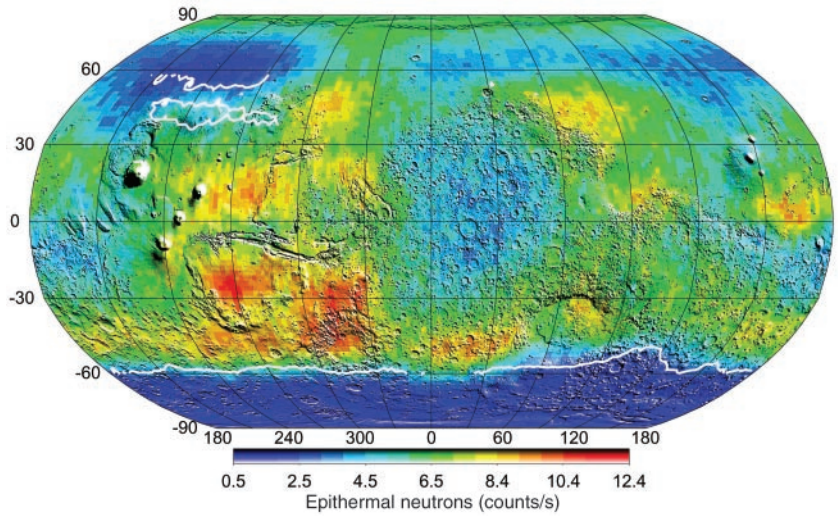

Fig. 6. Map of epithermal neutron flux from the Neutron Spectrometer. Low epithermal flux is indicative of high hydrogen concentration (*8*). Contours (in white) are shown of the regions where water ice is predicted to be stable at 80 cm depth (*21*) (no predictions were made poleward of 60° latitude because no data on thermal inertia were available). Note the correlation between regions of predicted ice stability and the low epithermal flux. The only exception is the small closed region of predicted ice stability, which is not observed in the epithermal neutron flux.

Water ice concentrations of 35 ± 15% by weight imply a subsurface material that is 60% (range from 40 to 73%) ice by volume, assuming a mean density for the non-ice component of 2.5 g/cm^3. The porosity of the upper meter of the martian soil is not well known. Estimates at the Viking Lander 1 site were 1.15 ± 0.15 g/cm^3 for drift material and 1.6 ± 0.4 g/cm^3 for blocky material (*22*). Assuming silicate grain densities of 2.5 g/cm^3 and absence of ice in the pores at the Viking 1 site, these inferred bulk densities yield porosities for these materials of 54 ± 6% and 36 ± 16%, respectively. The lower end of our inferred subsurface ice concentrations is consistent with these porosities if the pores are filled, but it is difficult to imagine a soil with sufficient porosity to accommodate an ice content toward the upper end of our inferred range.

It is important to note that we find a strong subsurface hydrogen signal on Mars essentially everywhere that ice is expected to be stable and where our signal is not obscured by CO_2. The total pore space in the regolith has been estimated to be sufficient to contain ice equivalent to a global water layer 0.5 to 1.5 km deep (*23*). Our results, of course, do not reveal anything about whether or not ice is present in the enormous volume of regolith that lies below the roughly 1 m depth to which the gamma and neutron techniques can sense. However, they certainly are consistent with the view that the subsurface regolith may be a substantial reservoir for martian water.

References and Notes

1. M. H. Carr, *Water on Mars* (Oxford Univ. Press, New York, 1996).
2. V. R. Baker, *Nature* **412**, 228 (2001).
3. H. H. Kieffer, S. C. Chase Jr., T. Z. Martin, E. D. Miner, F. D. Palluconi, *Science* **194**, 1341 (1976).
4. M. C. Malin, K. S. Edgett, *Science* **288**, 2330 (2000).
5. J. F. Mustard, C. D. Cooper, M. K. Rifkin, *Nature* **412**, 411 (2001).

6. W. V. Boynton *et al.*, *J. Geophys. Res.* **97**, 7681 (1992)
7. W. V. Boynton *et al.*, in preparation.
8. W. Feldman *et al.*, *Science* **297**, 75 (2002); published online 30 May 2002 (10.1126/science.1073541).
9. I. Mitrofanov *et al.*, *Science* **297**, 78 (2002); published online 30 May 2002 (10.1126/science.1073616).
10. W. V. Boynton, L. G. Evans, R. C. Reedy, J. I. Trombka, in *Remote Geochemical Analysis: Element and Mineralogical Composition*, C. M. Pieters, P. A. J. Englert, Eds. (Cambridge Univ. Press, New York, 1993), chap. 17.
11. W. C. Feldman, W. V. Boynton, D. M. Drake, in *Remote Geochemical Analysis: Element and Mineralogical Composition*, C. M. Pieters, P. A. J. Englert, Eds. (Cambridge Univ. Press, New York, 1993), chap. 10.
12. T. H. Prettyman *et al.*, *Lunar Planet. Sci. Conf.* **XXXIII** (abstr. 2012) (2002).
13. L. S. Waters, Ed., *MCNPX User's Guide* (document LA-UR-99-6058) (Los Alamos National Laboratory, Los Alamos, NM, 1999).
14. H. Wänke, J. Brückner, G. Dreibus, R. Rieder, I. Ryabchikov, *Space Sci. Rev.* **96**, 317 (2001)
15. K. Biemann *et al.*, *J. Geophys. Res.* **82**, 4641 (1977).
16. The exact H_2O content of the Viking soil does not have a strong influence on the conclusions of this work other than to change the composition of the upper layer in direct proportion to the Viking 1 H_2O content. The Viking 2 site was in a region far enough north that it appears to have abundant near-surface ice and, thus, cannot be used for normalization.
17. The statistics of the H gamma-ray line are not adequate to normalize to just one location on Mars, as was done for the neutron fluxes. The conclusions of this work are not sensitively dependent on the H gamma-ray normalization.
18. R. B. Leighton, B. C. Murray, *Science* **153**, 136 (1966).
19. C. B. Farmer, P. E. Doms, *J. Geophys. Res.* **84**, 2881 (1979).
20. D. A. Paige, K. D. Keegan, *J. Geophys. Res.* **99**, 26013 (1994).
21. M. T. Mellon, B. M. Jakosky, *J. Geophys. Res.* **98**, 3345 (1993).
22. H. J. Moore, B. M. Jakosky, *Icarus* **81**, 164 (1989).
23. S. W. Squyres, S. M. Clifford, R. O. Kuzmin, J. R. Zimbelman, F. M. Costard, in *Mars*, H. H. Kieffer, B. M. Jakosky, C. W. Snyder, M. S. Matthews, Eds. (Univ. of Arizona Press, Tucson, 1992), chap. 16.
24. We confirmed that the northern region is nearly opaque to gamma rays by noting that the signal from the radioactive element potassium in this region agreed with the signal determined during cruise to Mars within 4 ± 2%.

25. The authors would like to thank J. Astier, A. Evers, K. Crombie , G. Davidson, H. Enos, C. Fellows, M. Fitzgibbon, J. Hambleton, K. Harshman, D. Hill, K. Kerry, G. McArthur, C. Turner, M. Ward, and M. Williams of the University of Arizona for the hard work to design, build, test, calibrate, and operate the GRS. We also wish to thank the efforts of the Mars Odyssey project personnel at both the Jet Propulsion Laboratory and Lockheed Martin Astronautics for getting us safely to Mars.

8 May 2002; accepted 22 May 2002
Published online 30 May 2002;
10.1126/science.1073722
Include this information when citing this paper.

A New Skull of Early *Homo* from Dmanisi, Georgia

Abesalom Vekua,[1,2] David Lordkipanidze,[1]* G. Philip Rightmire,[3] Jordi Agusti,[4] Reid Ferring,[5] Givi Maisuradze,[1] Alexander Mouskhelishvili,[1,6] Medea Nioradze,[7] Marcia Ponce de Leon,[8] Martha Tappen,[9] Merab Tvalchrelidze,[6,10] Christoph Zollikofer[8]

Another hominid skull has been recovered at Dmanisi (Republic of Georgia) from the same strata in which hominid remains have been reported previously. The Dmanisi site dated to ~1.75 million years ago has now produced craniofacial portions of several hominid individuals, along with many well-preserved animal fossils and quantities of stone artifacts. Although there are certain anatomical differences among the Dmanisi specimens, the hominids do not clearly represent more than one taxon. We assign the new skull provisionally to *Homo erectus* (=*ergaster*). The Dmanisi specimens are the most primitive and small-brained fossils to be grouped with this species or any taxon linked unequivocally with genus *Homo* and also the ones most similar to the presumed *habilis*-like stem. We suggest that the ancestors of the Dmanisi population dispersed from Africa before the emergence of humans identified broadly with the *H. erectus* grade.

The new Dmanisi cranium (D2700) and associated mandible (D2735) were found in squares 60/65 and 60/66 (Fig. 1), embedded in the black to dark-brown tuffaceous sand immediately overlying the 1.85-million-year-old Masavera Basalt. Sedimentary horizons above the basalt also yielded two partial crania in 1999, along with mandibles discovered in 1991 and 2000 (*1*–*7*). The new hominid remains were associated with animal fossils that include an entire skull of *Stephanorhinus etruscus etruscus*, a skull of *Cervus perrieri* with a full rack of antlers, a *Dama nesti* antler, two crania of *Canis etruscus*, a complete mandible of *Equus stenonis*, and the anterior portion of a *Megantereon* cranium. Human occupation at Dmanisi is correlated to the terminal part of the (magnetically normal) Olduvai Subchron and immediately overlying (magnetically reversed) horizons of the Matuyama Chron, and is ~1.75 million years in age (*5*, *6*, *8*). Faunal remains also support the dating of Dmanisi to the end of the Pliocene or earliest Pleistocene (*8*, *9*).

The evidence suggests that much of the Dmanisi fauna was buried rapidly after death, in many cases with ligaments still attached, and that the bones were buried very gently, with minimal transport. The protection afforded the bones in lower layers by the overlying calcareous horizon halted further diagenetic damage and compaction that normally occur. Sedimentological information and the appearance of all the fossils found nearby reinforce the conclusion that the hominid and faunal remains were deposited in a brief interval. Seventy percent of the assemblage is in weathering stage 0 or 1, and none in stages 4 or 5 (*10*). Rapid, low-energy deposition was followed by formation of petrocalcic horizons higher in the section, which arrested further destruction of bone. We estimate that in the sample of over 3000 vertebrate faunal remains recovered thus far, about 30% of the specimens are unbroken, and almost 90% are identifiable to genus if not species.

The diversity and high proportion of carnivores in the assemblage are paralleled by some tooth pits and characteristic carnivore breakage patterns, and also some hyena coprolites, but the general character of the assemblage in many ways does not fit conceptions of carnivore lairs (*11*).

The mammalian fauna includes new rodent species, which confirm that Dmanisi predates the holarctic dispersal of rootless voles (*Allophaiomys-Microtus* group). We also found a large, archaic *Mimomys*, which fits well in the *Mimomys pliocaenicus* group from the late Pliocene (Villanyian biozone) in European sites (Tegelen in the Netherlands, Val d'Arno in Italy, East and West Runton in England), a smaller vole of the *Tcharinomys* (*Pusillomimus*) lineage, abundant gerbils (*Parameriones* sp.), and hamsters (*Cricetus* sp., *Allocricetus bursae*) (*12*).

Stone artifacts were found throughout the sediment section, but, as in the previously

[1]Georgian State Museum, Georgian Academy of Sciences, 3 Purtseladze Street, Tbilisi 380007, Georgia. [2]Institute of Paleobiology, Georgian Academy of Sciences, Niagvris 4A, Tbilisi 380004, Georgia. [3]Department of Anthropology, Binghamton University (State University of New York), Binghamton, NY 13902, USA. [4]Institut de Paleontologia M. Crusafont, 08201-Sabadell, Spain. [5]Department of Geography, University of North Texas, Denton, TX 76203, USA. [6]Institute of Geography, Georgian Academy of Sciences, M. Alexidze 1, Tbilisi 380093, Georgia. [7]Archeological Center, Georgian Academy of Science, 14 Uznadze Street, Tbilisi 380002, Georgia. [8]Anthropological Institute and MultiMedia Laboratory, Universität Zürich-Irchel, 190 Winterthurerstrasse, CH-8057 Zürich, Switzerland. [9]Department of Anthropology, University of Minnesota, Minneapolis, MN 55455, USA. [10]Institute of Geology of Georgian Academy of Sciences, M. Alexidze 1, Tbilisi 380093, Georgia.

*To whom correspondence should be addressed. E-mail: geonathist@ip.osgf.ge